PAPER

Near-field absorption imaging by a Raman nano-light source

Ryo Kato,[a] Yuika Saito*[ab] and Prabhat Verma[a]

In aperture-less near-field scanning optical microscopy (NSOM), when the apex of a sharp silicon nano-tip is illuminated with an incident laser, the Raman scattered signal from silicon creates a nano-light source with a wavelength the same as the LO phonon mode of silicon. This Raman scattered light can be absorbed by a sample placed under the tip and thus enables us to study the optical properties of the sample at the nano-scale through the absorption of silicon Raman scattered light. In this study, we demonstrate nano-scale absorption imaging by measuring the intensity of silicon Raman signals generated at the apex of a near-field probe under a platform of conventional NSOM. We used two incident lasers of different colors, which allowed the absorption properties of the sample to be observed independent of topography, revealing the inherent optical properties of the sample. The present results demonstrate the flexibility of aperture-less NSOM, not only for vibrational spectroscopies, such as tip-enhanced Raman spectroscopy, but also for electronic energy state analysis, which is achieved by monitoring the intensity of the Raman nano-light source rather than the Rayleigh scattering. This new method of near-field imaging can extend the potential applications of aperture-less NSOM.

1. Introduction

At present, near-field scanning optical microscopy (NSOM) is the only visible light based spectroscopic technique with nanoscale resolution. In particular, with aperture-less NSOM, spatial resolution as low as a few nanometers has been achieved using strong field localization at the apex of sharp probes.[1–3] Aperture-less NSOM was first developed for Rayleigh scattering,[4] followed by Raman spectroscopy,[5,6] nonlinear Raman spectroscopy,[7] photoluminescence,[8] and two-photon fluorescence.[9] The versatility of aperture-less NSOM has been primarily established for Raman spectroscopy, more specifically, tip-enhanced Raman spectroscopy (TERS), and has helped reveal local inhomogeneities in semiconductors,[10] carbon materials,[11–15] polymers,[16] and biological substances.[17,18] In principle, aperture-less NSOM can be employed in a variety of spectroscopic applications, *e.g.*, the absorption and scattering of molecules for electronic state analysis, as well as vibrational spectroscopy *via* monitoring of the Rayleigh scattering efficiency.[19,20] However, understanding the image contrast originating from Rayleigh scattering is a complex problem since the background signal from the substrate and the optics cannot be separated from the signal generated by the sample. Moreover, the effect of sample volume must be eliminated in order to obtain the inherent optical properties of the sample. This

problem never arises in TERS, because the Raman signal essentially corresponds to only the intrinsic frequencies of the sample. Therefore, conducting electronic state analysis is not straightforward using conventional aperture-less NSOM.

In this study, we present a nano-scale absorption imaging method using aperture-less NSOM to complement TERS data by providing the local absorption efficiency of a sample. This method is similar to conventional TERS but relies on a novel Raman-nano-light source that is created by the Raman scattering from a near-field tip made of silicon, which is simultaneously excited by two lasers of different colors.

The nano-scale absorption imaging setup used in the present study is illustrated in Fig. 1. A strong Raman signal generated at the apex of a near-field silicon probe acted as a nano-light source during near-field imaging. In TERS, a metal-coated tip is utilized as the near-field probe for excitation of a localized surface plasmons, which results in the confinement and enhancement of light field at the apex.[21,22] However, even if one employs a bare silicon tip (*i.e.*, not coated with any metal), a strong light confinement can be obtained at the apex of the tip. In the case of a bare silicon tip, bringing the tip into the focal point results not only the sample signal, but also the Raman scattering of silicon originating from the apex of the silicon tip.[23] In this study, we employed two different excitation lasers with wavelengths of 488 and 594 nm. The wavelength of the nano-light source is shifted by 520 cm^{-1} (LO mode of silicon) relative to that of each excitation laser and this Raman scattering of silicon is detected through the sample. Since part of the transmitted Raman light is absorbed by the sample, one

[a]*Department of Applied Physics, Osaka University, Suita, Osaka, 565-0871 Japan*
[b]*Department of Chemistry, Gakushuin University, Mejiro, Toshima, Tokyo 171-0031, Japan. E-mail: yuika.saito@gakushuin.ac.jp; Tel: +81-3-5904-9381*
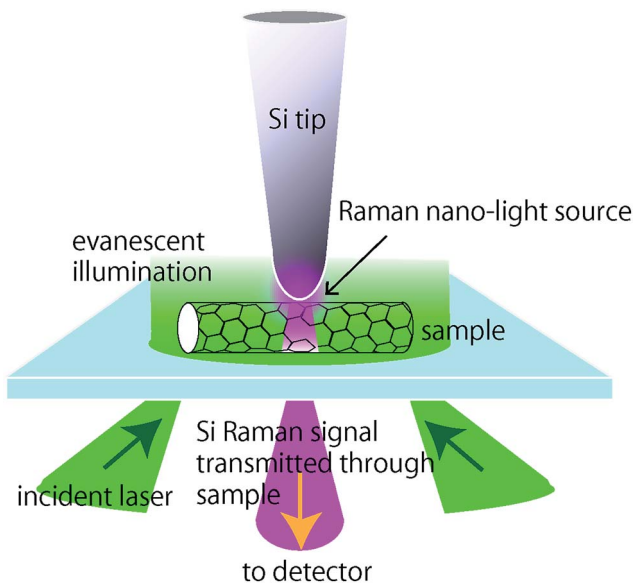
Fig. 1 Schematic illustration of nano-scale absorption imaging. Raman scattered light generated at the apex of a silicon tip is obscured when it is transmitted through the sample. Evanescent light enables the illumination of the tip apex alone with the incident light, which provides high spatial resolution corresponding to the size of the tip apex.
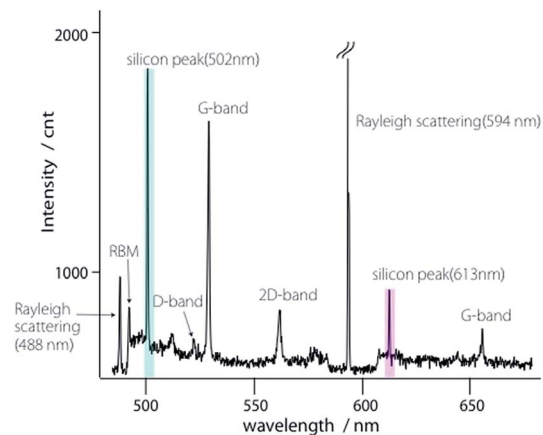

Fig. 2 Raman spectrum showing vibrational modes of both silicon and sample (CNTs) obtained simultaneously with 488 nm and 594 nm lasers. The blue and pink hatch indicates the silicon peak at 502 nm and 613 nm respectively.

can obtain an image of the sample absorption by monitoring the transmuted intensity of the silicon Raman light. This method extends the ability of conventional TERS, which only characterizes the vibrational properties of the sample. When evanescent illumination is used, only the apex of the nano-tip is irradiated with the excitation light, which results in high spatial resolution corresponding to the size of the tip apex (typically 3–10 nm in diameter). In the present experiment, by employing two excitation lasers, any topographic artifact originating from the movement of near-field probe in the z direction is eliminated.[24,25] Moreover, the absorption spectra can be obtained through multi-color measurements. Unlike in Rayleigh scattering, the origin of the detected signal is likely to be at the apex of the probe, therefore, better stability and precision can be achieved using this novel light source. As an example, we demonstrate that carbon nanotubes with different absorption efficiencies could be clearly distinguished by this new technique.

2.   Results and discussion

The present optical setup for nano-scale absorption imaging was similar to the previously reported TERS system[26] (see the Experimental section).

Fig. 2 shows the Raman spectrum of the silicon tip and the semiconducting CNTs. The peak at 502 nm is assigned to the LO-vibrational mode of silicon generated by 488 nm excitation, while the peak at 613 nm is also the LO-mode of silicon generated by 594 nm excitation. Several vibrational modes that originate from CNTs, *e.g.*, RBM, D and G, and 2D bands, are also observed for the two excitation lasers.[27–30] The Raman signals

generated by the 488 nm laser exhibited higher intensities than those generated by the 594 nm laser, primarily due to the wavelength dependence of the scattering efficiency.

Fig. 3(a) shows an AFM image of the sample after only metallic CNTs were casted on the glass substrate, while Fig. 3(b) shows an AFM image after both metallic and semiconducting CNTs were casted. A comparison of the two AFM images helps in identifying the two kinds of CNTs. Fig. 3(c) is an AFM image of a small area of the sample that contains two types of CNT bundles, metallic (m-CNT, left-hand side) and semiconducting (s-CNT, right-hand side). Near-field absorption images corresponding to the AFM scan area are shown in Fig. 3(d) and (e). In both figures, two bundles of CNTs were observed with a spatial resolution as high as ~20 nm. The images were constructed using the intensities of the silicon Raman signals measured at 502 nm (d) and 613 nm (e). The signal intensity was normalized
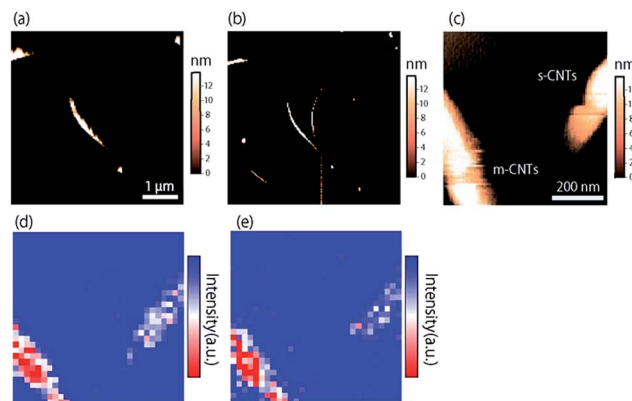

Fig. 3 (a) AFM image of the sample containing only m-CNT (b) AFM image of the same sample after casting both m-CNTs and s-CNTs. (c) AFM image of a small area containing two bundles of CNTs. The CNT bundle on the left-hand side is metallic, while that on the right-hand side is semiconducting. Absorption images of the CNT samples, obtained from the intensities of silicon Raman scattering at $\omega = 502$ nm (d) and $\omega = 613$ nm (e).

with the intensity when the tip was placed on the glass substrate. As explained in Fig. 1, the signal intensity of Raman scattering from silicon decreased when the tip was on the CNTs, as compared to when it was away from the CNTs. In Fig. 3(d) and (e), however, the presence of any topographic variation also contributed to the contrast. Although the CNTs in the left-hand and right-hand sides of Fig. 3(c) are of different types, the contrasts in Fig. 3(d) and (e) are similar. According to the AFM image, the CNT bundle on the left-hand side was thicker (13 nm) than the one on the right-hand side (10 nm). The thicker bundle also exhibited higher contrast in the optical images.

For further analysis, it is instructive to examine the physical parameters related to absorption. The absorbance A can be expressed as follows:[31]

$$A = \varepsilon c L, \tag{1}$$

where ε is the absorption coefficient specific to the sample, c is the molecular concentration, and L is the sample thickness. Eqn (1) indicates that the total amount of absorption depends on both L and c. Thus, a comparison between Fig. 3(d) and (e) will reveal accurate information regarding ε, which corresponds to the sample properties. Since both A_{613} and A_{502} would be ideally zero at the locations where there is no sample, the ratio of the two quantity would have an arbitrary value including infinity. In order to avoid the division of zero by zero, we exclude the locations where there is no sample from the data analysis, and set the data value at these points to be 1. We would also like to add here that the sample always provides a finite value even when the absorption at 502 nm is weak. According to eqn (1), this ratio depends only on the absorption coefficient of the sample, so it is independent of the sample concentration and thickness. The effect of the sample topography can thus be eliminated, as indicated in eqn (2):

$$\frac{A_{613}}{A_{502}} = \frac{\varepsilon_{613}}{\varepsilon_{502}}. \tag{2}$$

As expected, two types of CNTs can clearly be distinguished in Fig. 4(a). Unlike in Fig. 3(d) and (e), the image in Fig. 4(a) was independent of the sample topography, and therefore reflects

the pure optical properties of the sample. As estimated from the height obtained from the AFM image, both CNTs that appear in Fig. 3(c) consist of bundles. The fluctuations observed within each bundles in Fig. 4(a) presumably stem from the variation of energy levels of each nanotube due to the interactions between adjacent nanotubes or due to a possible variation in their diameters. The spatial resolution was evaluated from the FWHM of the line profile along the white dotted line in Fig. 4(a), shown in the inset, which was estimated to be as high as 18 nm. Because CNTs are highly absorptive, we believe that the cause of the contrast is near-field absorption. In this study, the interference phenomena, reported in ref. 32 under a far-field microscope, were less dominant.

Fig. 4(b) shows the normalized UV-Vis absorption spectra of the m-CNTs and s-CNTs, dispersed in 1,2-dichloroethane. The black dotted lines indicate the absorbance at 502 nm and at 613 nm respectively, both of which correspond to the silicon Raman signal. The m-CNTs exhibit higher absorption at 613 nm as compared to 502 nm, whereas the s-CNTs exhibit higher absorbance at 502 nm in comparison to 613 nm. Accordingly, in Fig. 4(a), the absorbance ratio A_{613}/A_{502} is higher for m-CNT (left) than s-CNT (right), in agreement with the UV-Vis spectra. According to Fig. 4(a), the average absorption ratios are 1.08 ± 0.25 and 0.74 ± 0.16 for the left and the right nanotubes, respectively. On the other hand, in Fig. 4(b), the corresponding ratios are 1.14 and 0.87 for the left and the right nanotubes, respectively. The slight differences in the ratio values in the two figures may come from the difference in experimental conditions, where the former was obtained from an individual bundle placed on a glass substrate in air, while the later was obtained from multiple nanotubes dissolved in a solution.

The spectroscopic sensitivity in this technique is much higher due to the direct irradiation of the probe by a tightly focused excitation laser. Moreover, the throughput of an optical fiber, especially in aperture NSOM, is quite sensitive to the excitation wavelength, although for electronic state analysis of molecules, it is essential to use a wide wavelength range. The Raman signal from silicon can be detected from the ultraviolet to the infrared,[33] and a silicon tip is compatible with a variety of Raman spectroscopic systems. Thus, our method can be applied for a wide range of samples and for a variety of experimental setups. The only restriction is the throughput of the objective lens of the microscope, which is used to focus the incident laser and collect the Raman signal. The multi-colorization is the key to extend the capability of nano-scale absorption imaging for future applications. This can be realized by employing a spectroscopic system, which could cover the entire visible wavelength range, e.g., an echelle spectrometer equipped with a large-pixel CCD camera. Theoretically there is no limitation for the sample thickness, however, practically the sample should be thin enough to create a Si-Raman-light-source at the tip apex via evanescent illumination.
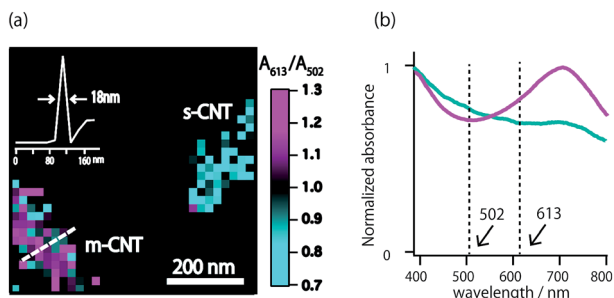

Fig. 4 (a) Nano-scale absorbance image of CNTs constructed from the data in Fig. 3(d) and (e). The inset shows a line profile along the dotted line. (b) Normalized UV-Vis absorption spectrum of metallic (pink) and semiconducting (blue) CNTs. The black dotted lines indicate the absorbance at 502 and 613 nm, respectively.

3. Conclusion

We demonstrated nano-scale near-field absorption imaging by measuring the intensity of silicon Raman signals emanating

from the apex of a near-field probe made of silicon that transmits through a sample under the tip. In this measurement, a bare silicon tip plays the role of a novel nano-light source for aperture-less NSOM, which provides us with high spatial resolution, far beyond the diffraction limit of light, similar to that in a conventional near-field microscope. Since the intensity of the Raman signal of silicon decreases after passing through a sample, optical absorbance of the sample can be imaged by this technique. Unlike in Rayleigh scattering, the excitation light for absorption measurements originates only from the tip apex, therefore more precise and stable analysis can be achieved. Employing two lasers of different colors enabled us to observe the absorption coefficient independent of the sample topography and molecular concentration.

The success of our nano-imaging technique was verified by the absorption ratio image of CNT bundles, from which two types of nanotubes were clearly distinguished. The optical setup is based on conventional aperture-less NSOM and thus can be combined with other imaging technique such as TERS using a metal-coated tip. The combination of near-field absorption and Raman analysis will provide new possibilities for nano-scale analysis of both electronic and vibrational properties. Moreover, multi-colorization will be critical in extending the applicability of the technique, *e.g.*, to band-gap imaging of semiconductor materials, nano-imaging of biomaterials, and polymer films.

4. Experimental

Optical measurement

The output beams of the two diode lasers used for Raman excitation were passed through 10× beam expanders and converted to radial polarization. An optical mask was inserted into the incident laser path in order to generate purely evanescent light at the surface of the glass substrate on which the sample was placed. Both excitation lasers were focused through a high-NA oil-immersion microscope objective lens (60×, NA = 1.4) and the Raman signal was collected by the same lens. In the present measurement setup, the near-field probe tip was a commercially available silicon cantilever (OMCL-AC240TN-C3) used in atomic force microscopy (AFM; NanoWizard3, JPK Inst.). This silicon tip was not coated with any metal, as is usually done in aperture-less near-field microscopy. Two notch filters were inserted into each output path to cut out the Rayleigh scattering light, and an additional aperture mask was inserted to reject the NA >1 components of the signal, which included mainly reflected light from the glass substrate. The output signal was guided to a single spectrometer and was detected by a peltier-cooled charge coupled device (CCD) camera. The slit width of the spectrometer was set to 100 μm and the grating was 150 lines per cm, which was wide enough to cover Raman signals originating from the two excitation lasers.

Absorption imaging was conducted in a similar manner as TERS. The near-field probe was brought into the focal point, and Raman signals of the sample and silicon were collected. Absorption measurements were performed with an exposure time of 3.0 s at each pixel, and images were obtained from a 600 × 600 nm^2 area (step size: 20 nm) with a resolution of 30 square pixels. The power of both excitation lasers was set to 0.2 mW. An AFM image of the sample was taken of the same area to confirm the sample topography.

The absorption spectra of CNT solutions were obtained using a UV-Vis spectrometer (SHIMADZU/UV-3600). Spectra were normalized by the maximum intensity.

Sample preparation

In order to prepare the CNT sample, we dissolved commercially available CNTs (NanoIntegris, IsoNanotubes-M/IsoNanotubes-S) in 1,2-dichloroethane through a 30 min sonication. The solution was then dropped on a glass substrate and spin-coated. The sample thus prepared contained small bundles of CNTs. Finally, we coated the CNTs with osmium to prevent them from being scratched by the AFM tip during scanning. To confirm the presence of two types of CNTs, we first spin-coated only metallic CNTs, obtained an AFM image of the sample, then spin-coated semiconducting CNTs on the same substrate, and obtained another AFM image of the same area. By comparing the two AFM images, we identified the two types of CNTs.

Acknowledgements

References

1 J. Yu, Y. Saito, T. Ichimura, S. Kawata and P. Verma, *Appl. Phys. Lett.*, 2013, **102**, 123110.

2 M. Liao, S. Jiang, C. Hu, R. Zhang, Y. Kuang, J. Zhu, Y. Zhang and Z. Dong, *Nano Lett.*, 2016, **16**, 4040.

3 S. Jiang, Y. Zhang, R. Zhang, C. Hu, M. Liao, Y. Luo, J. Yang, Z. Dong and J. G. Hou, *Nat. Nanotechnol.*, 2015, **10**, 865.

4 Y. Inouye and S. Kawata, *Opt. Lett.*, 1994, **19**, 159.

5 N. Hayazawa, Y. Inouye, Z. Sekkat and S. Kawata, *Chem. Phys. Lett.*, 2001, **335**, 369.

6 R. M. Stockle, Y. D. Suh, V. Deckert and R. Zenobi, *Chem. Phys. Lett.*, 2000, **318**, 131.

7 T. Ichimura, N. Hayazawa, M. Hashimoto, Y. Inouye and S. Kawata, *Appl. Phys. Lett.*, 2004, **84**, 1768.

8 A. Hartschuh, H. Qian, A. J. Meixner, N. Anderson and L. Novotny, *Nano Lett.*, 2005, **5**, 2310.

9 N. Hayazawa, K. Furusawa, A. Taguchi, S. Kawata and H. Abe, *Appl. Phys. Lett.*, 2009, **94**, 193112.

10 Y. Saito, M. Motohashi, N. Hayazawa, M. Iyoki and S. Kawata, *Appl. Phys. Lett.*, 2006, **88**, 143109.

11 N. Peica, C. Thomsen and J. Maultzsch, *Phys. Status Solidi B*, 2010, **247**, 2818.

12 T. Yano, Y. Inoue and S. Kawata, *Nano Lett.*, 2006, **6**, 1269.

13 Y. Okuno, Y. Saito, S. Kawata and P. Verma, *Phys. Rev. Lett.*, 2013, **111**, 216101.

14 T. Yano, P. Verma, Y. Saito, T. Ichimura and S. Kawata, *Nat. Photonics*, 2009, **3**, 473.

15 T. Yano, T. Ichimura, S. Kuwahara, F. H'Dhili, K. Uetsuki, Y. Okuno, P. Verma and S. Kawata, *Nat. Commun.*, 2013, **10**, 3592.

16 T. Suzuki, X. Yan, Y. Kitahama, H. Sato, T. Itoh, T. Miura and Y. Ozaki, *J. Phys. Chem. C*, 2013, **117**, 1436.

17 E. Bailo and V. Deckert, *Angew. Chem.*, 2008, **47**, 1658.

18 G. Rusciano, G. Zito, R. Isticato, T. Sirec, E. Ricca, E. Bailo and A. Sasso, *ACS Nano*, 2014, **8**, 12300.

19 C. Casiraghi, A. Hartschuh, E. Lidorikis, H. Qian, H. Harutyunyan, T. Gokus, K. S. Novoselov and A. C. Ferrari, *Nano Lett.*, 2007, **7**, 2711.

20 D. Y. Joh, L. H. Herman, S. Y. Ju, J. Kinder, M. A. Segal, J. N. Johnson, G. K. L. Chan and J. Park, *Nano Lett.*, 2011, **11**, 1.

21 N. Hayazawa, T. Yano, H. Watanabe, Y. Inouye and S. Kawata, *Chem. Phys. Lett.*, 2003, **376**, 174.

22 M. D. Sonntag, J. M. Klingsporn, L. K. Garibay, J. M. Roberts, J. A. Dieringer, T. Seideman, K. A. Scheidt, L. Jensen, G. C. Schatz and R. P. Van Duyne, *J. Phys. Chem. C*, 2012, **116**, 478.

23 Y. Saito, P. Verma, K. Masui, Y. Inouye and S. Kawata, *J. Raman Spectrosc.*, 2009, **40**, 1434.

24 M. Labardi, S. Patane and M. Allegrini, *Appl. Phys. Lett.*, 2000, **77**, 621.

25 B. Hecht, H. Bielefeldt, Y. Inouye, D. W. Pohl and L. Novotny, *J. Appl. Phys.*, 1997, **81**, 2492.

26 T. Mino, Y. Saito and P. Verma, *ACS Nano*, 2014, **8**, 10187.

27 M. S. Dresselhaus, G. Dresselhaus, A. Jorio, A. G. Souza Filho and R. Saito, *Carbon*, 2002, **40**, 2043.

28 A. Jorio, M. A. Pimenta, A. G. Souza Filho, R. Saito, G. Dresselhaus and M. S. Dresselhaus, *New J. Phys.*, 2003, **5**, 139.

29 T. Yano, P. Verma and S. Kawata, *Appl. Phys. Lett.*, 2006, **88**, 093125.

30 C. Georgi and A. Hartschuh, *Appl. Phys. Lett.*, 2010, **97**, 143117.

31 W. G. Zijlstra, A. Buursma and O. W. van Assendelft, *Visible and near infrared absorption spectra of human and animal haemoglobin: determination and application*, VSP, Utrecht, Boston, 2000.

32 K. Lindfors, T. Kalkbrenner, P. Stoller and V. Sandoghdar, *Phys. Rev. Lett.*, 2004, **93**, 037401.

33 A. Ogura, D. Kosemura, M. Takei, H. Uchida, N. Hattori, M. Yoshimaru, S. Mayuzumi and H. Wakabayashi, *Mater. Sci. Eng., B*, 2009, **159**, 206.